Chapter 5: Modeling of the isotopic composition of stratospheric sulfur species

5.1 Introduction

Isotopic data provides an additional constraint on the sulfur sources to the SSA layer. In this regard, we have estimated the relative isotopic enrichments of the major production pathways for the SSA and measured the sulfur isotopic composition of the SSA particles. We concluded in Chapter 2 [*Leung et al.*, 2002] that the sulfur isotopic enrichment factor obtained from our analysis of high-resolution FTIR balloon data was inconsistent with biogenic OCS being the primary contributor to stratospheric sulfate aerosol, in contrast to recent reports of OCS being the principal sulfur source, along with SO_2 and tropospheric sulfate [*Leung et al.*, 2002]. However, in Chapter 2, we assumed that $\delta^{34}S \sim 0$ ‰ for SSA derived from SO_2. This assumption may be not valid.

For example, the isotopic enrichment during the association of SO_2 and OH, which is the rate determining step in the homogeneous gas-phase oxidation of SO_2 by OH has a large, positive value (Chapter 4 and [*Leung et al.*, 2001]) that is consistent with the earlier experimental results of Castleman et al. [*Castleman et al.*, 1973; *Castleman et al.*, 1974]. The heterogeneous oxidation of SO_2 to SO_4^{2-} likewise has a positive, albeit smaller, value for ε. This result highlights the need to consider the isotopic effect of all the sulfate production pathways.

The apparent enrichment factor, $\varepsilon_{apparent}$, for OCS processing in the stratosphere will in fact be smaller than the actual enrichment factor during photolysis, $\varepsilon_{photolysis}$, due to diffusive effects. In addition, two other loss pathways for OCS (i.e., oxidation by OH and O) are operative in the stratosphere. As a consequence, the $\varepsilon_{apparent}$ represents a weighted isotopic enrichment factor for the sum of these processes, although the decrease

in P_{OCS} with altitude is consistent with photolytic dissociation as the primary loss pathway.

The isotopic enrichment factor for OCS photolysis is wavelength dependent and varies throughout the stratosphere depending on the solar UV flux at a given altitude. Furthermore, the relative importance of the oxidation pathways involving O and OH lead to further uncertainties. In order to address this problem, we estimated in Chapter 3 the wavelength-dependent isotopic enrichment of OCS photolytic decomposition from the absorption spectra of the isotopologues $OC^{32}S$ and $OC^{34}S$.

In this chapter, we employed Caltech/JPL KINETICS CTM (chemical transport model) in 1-D mode combined with the gas-phase sulfur isotope chemistry to explore the steady-state isotopic compositions of OCS, SO_2 and SSA.

5.2 Atmospheric simulation

The Caltech/JPL KINETICS CTM was used in the 1-D standard earth model mode at typical mid-latitude conditions [*Allen et al.*, 1981]. The model atmosphere is divided into 66 uniformly distributed and fixed boxes as a function of altitude over 130 km. In our calculations, the tropopause is set at 14 km. The model calculations were run to steady-state over 10 years using input data which are described in the appendices.

The set of chemical reactions used for sulfur species generally follows *DeMore et al.* [1997] and *Weisenstein et al.* [1997] [*DeMore et al.*, 1997; *Weisenstein et al.*, 1997]. The complete list of sulfur containing species and reactions can be found in Table 5.1 and 5.2, respectively. Short-lived sulfur-containing radical intermediates were explicitly modeled. All other species, including OH and O, and NO_3 were held constant at typical

atmospheric values. ^{32}S and ^{34}S isotopologues were treated as separate species with parallel sets of reactions. All compounds were assumed to have two S-isotopologues, with the exception of CS_2, which had three: $C^{32}S_2$, $C^{34}S_2$ and $C^{32}S^{34}S$. All of the species listed in Table 5.1 and the given reactions in Table 5.2 have duplicate entries, one for the ^{32}S isotopologue, and the other for the ^{34}S isotopologue. Again, the exception is for reactions involving CS_2. The isotopic compositions of the sulfur species were estimated from the values given by *Krouse and Grinenko* [1991].

Boundary conditions for major sulfur species (Table 5.1) expressed either as surface fluxes or as surface mixing ratios, were taken from *Weisenstein et al.* [1997]. The initial values of all other species were set to zero and allowed to evolve to a steady-state condition.

For the oxidation pathway involving SO_2 oxidation by OH, the isotopic enrichment factors determined by *Leung et al.* [2001] were used. As a simplifying assumption, all other chemical reaction rates were considered to be unaffected by isotopic substitution.

Table 5.1: Boundary conditions used in the Caltech/JPL I-D model

Species	Boundary condition	Boundary Value
SO_2	Surface flux	7.2×10^{9}
H_2S	surface mixing ratio	3.0×10^{-11}
OCS	surface mixing ratio	5.0×10^{-10}
CS_2	surface flux	4.6×10^{91}
CH_3SCH_3	surface flux	3.3×10^{8}
S H_2SO_4 SO SO_3 SH SO HSO_2 HSO_3 CS HCS CH_2SO CH_3S CH_3S CH_3SO CH_3SO_2 CH_3SCH_2	No boundary conditions set	

Surface flux is given in $cm^{-2}s^{-1}$

The above boundary conditions were used by Weisenstein et al. (1997).

Table 5.2: Sulfur reaction set used in 1-D and 2-D model

Reaction	*Rate Constant*
$O + CS \rightarrow CO + S$	$2.70 \times 10^{-10}\, e^{-760/T}$
$O + H_2S \rightarrow OH + SH$	$9.20 \times 10^{-12} e^{-1800/T}$
$O + OCS \rightarrow SO + CO$	$2.10 \times 10^{-11} e^{-2200/T}$
$O + CS_2 \rightarrow SO + CS$	$3.20 \times 10^{-11} e^{-650/T}$
$O + CH_3SCH_3 \rightarrow CH_3SO + CH_3$	$1.30 \times 10^{-11}\, e^{410/T}$
$O + SO_2 + M \rightarrow SO_3 + M$	$k_o = 1.30\times 10^{-33}(T/300)^{3.6}$
	$k_\infty = 1$
$O_2 + CS \rightarrow OCS + O$	2.90×10^{-19}
$O_3 + CS \rightarrow OCS + O_2$	3.00×10^{-16}
$OH + SO_2 + M \rightarrow HSO_3 + M$	$k_0 = 3.00 \times 10^{-31}(T/300)^{-3.3}$
	$k_\infty = 1.5 \times 10^{-12}$
$OH + H_2S \rightarrow SH + H_2O$	$6.00 \times 10^{-12} e^{-75/T}$
$OH + OCS \rightarrow SH + CO_2$	$1.10 \times 10^{-13} e^{-1200/T}$
$OH + S \rightarrow H + SO$	6.60×10^{-11}
$OH + CS_2 \rightarrow SH + OCS$	1.50×10^{-15}
$OH + CH_3SCH_3 \rightarrow 2H_2CO + SO_2 + Products$	$1.20 \times 10^{-11}\, e^{-260/T}$
$NO_2 + CS \rightarrow OCS + NO$	7.60×10^{-17}
$NO_3 + CH_3SCH_3 \rightarrow CH_3SCH_2 + HNO_3$	$1.90 \times 10^{-13}\, e^{500/T}$
$Cl + H_2S \rightarrow SH + HCl$	$3.70 \times 10^{-11}\, e^{210/T}$
$Cl + CH_3SCH_3 \rightarrow CH_3SCH_2 + HCl$	2.50×10^{-10}
$ClO + CH_3SCH_3 \rightarrow CH_3SCH_2 + HOCl$	9.50×10^{-15}
$S + O_2 \rightarrow SO + O$	2.30×10^{-12}
$S + O_3 \rightarrow SO + O_2$	1.20×10^{-11}
$S + OH \rightarrow SO + H$	6.60×10^{-11}
$SO + O_2 \rightarrow SO_2 + O$	$2.60 \times 10^{-11}\, e^{-2400/T}$
$SO + O_3 \rightarrow SO_2 + O_2$	$3.60 \times 10^{-12}\, e^{-1100/T}$
$SO + OH \rightarrow SO_2 + H$	8.60×10^{-11}
$SO + NO_2 \rightarrow SO_2 + NO$	1.40×10^{-11}
$SO + ClO \rightarrow SO_2 + Cl$	2.80×10^{-11}
$SO + OClO \rightarrow SO_2 + ClO$	1.90×10^{-12}
$SO_3 + H_2O \rightarrow H_2SO_4$	2.40×10^{-15}
$SH + O \rightarrow H + SO$	1.60×10^{-10}
$SH + O_2 \rightarrow OH + SO$	4.00×10^{-19}
$SH + O_3 \rightarrow HSO + O_2$	$9.00 \times 10^{-12}\, e^{-280/T}$
$SH + NO_2 \rightarrow HSO + NO$	$2.90 \times 10^{-11}\, e^{240/T}$
$HSO + O_3 \rightarrow SH + 2O_2$	7.00×10^{-14}
$HSO + O_3 \rightarrow HSO_2 + O_2$	3.00×10^{-14}
$HSO + NO_2 \rightarrow HSO_2 + NO$	9.60×10^{-12}
$HCS + O_2 \rightarrow SO_2 + Products$	1.00×10^{-10}
$HSO_2 + O_2 \rightarrow HO_2 + SO_2$	3.00×10^{-13}
$HSO_3 + O_2 \rightarrow HO_2 + SO_3$	$1.30 \times 10^{-12}\, e^{-330/T}$
$CH_3S + O_2 \rightarrow CH_3SO_2$	3.00×10^{-18}
$CH_3S + O_3 \rightarrow CH_3O + SO_2$	$1.70 \times 10^{-12}\, e^{290/T}$
$CH_3S + O_3 \rightarrow CH_3SO + O_2$	$3.00 \times 10^{-13}\, e^{290/T}$
$CH_3S + NO_2 \rightarrow CH_3SO + NO$	$2.10 \times 10^{-11}\, e^{320./T}$
$CH_3SO + O_3 \rightarrow CH_2SO + OH + O_2$	3.00×10^{-13}
$CH_3SO + O_3 \rightarrow CH_3S + 2O_2$	3.00×10^{-13}
$CH_3SO + NO_2 \rightarrow SO_2 + NO + CH_3$	1.20×10^{-11}
$CH_3SO_2 + NO \rightarrow CH_3SO + NO_2$	1.10×10^{-11}
$CH_3SO_2 + NO_2 \rightarrow CH_3SO + NO_3$	2.20×10^{-11}
$CH_3SCH_2 + NO_3 \rightarrow HCS + HNO_3 + CH_3$	3.00×10^{-10}
$CH_2SO + M \rightarrow H_2CO + SO_2$	
$CH_3SO_2 + M \rightarrow CH_3S + O_2 + M$	

Bimolecular rate constants are expressed in molecules cm^{-3} s^{-1}. Rate constants for three-body reactions are in units of molecules^2 cm^{-6} s^{-1}. Temperature is in units of K.

UV-absorption cross-sections for $OC^{32}S$ at 225K and 295K were taken from *DeMore et al.* [1997]. Corresponding values for the $OC^{34}S$ absorption cross-sections in the region between 205 and 250 nm were calculated using the wavelength-dependent enrichment factors from *Colussi et al.*, [2002]. Even though there may be significant uncertainties associated with the values determined in this work, (see Chapter 3) the values we use were "anchored" on the apparent stratospheric sulfur isotopic enrichment factor ε determined from the MkIV FT-IR data [*Leung et al.*, 2002], as discussed below. For the remainder of the spectrum, a constant enrichment factor $(\alpha-1) = 73$ ‰ obtained from the *Leung et al.* [2002] was used. Sensitivity analyses confirm that the program is insensitive to changes in the OCS absorption spectrum outside the 205-250 nm region, where UV intensity in the stratosphere is minimal.

The quantum yield for OCS photolysis was assumed to be unity over the entire UV spectrum. This assumption was also made by *Weisenstein et al.* [1997] on the basis of *Zhao et al.* [1995]. However, we did not include the photolysis of H_2SO_4 and SO_3, which were considered in by *Weisenstein et al.* [1997]. The partitioning of these species is treated as a function of altitude. Below 30 km, H_2SO_4 and SO_3 are found primarily in the aerosol phase [*Burkholder et al.*, 2000]. Therefore, these reactions, which are of importance in the middle and upper stratosphere are of much less importance in the lower stratosphere.

A parameterized rate constant for the washout of $SO_{2(g)}$ and $H_2SO_{4(g)}$ was included in the troposphere and represents a range of loss processes which are not treated explicitly, such as heterogeneous chemical reactions. Eddy diffusion coefficients (K_{zz}) reflect the cumulative effects of a variety of transport processes. Loss of gaseous H_2SO_4

to stratospheric sulfate aerosol was modeled as a unimolecular loss process using the the mass transfer coefficient of H_2SO_4 in air calculated at 200 K [*Widmann and Davis*, 1997], and aerosol surface area densities approximated from values recommended by the WMO for calculations of heterogeneous ozone chemistry [*Weisenstein et al.*, 1997].

The OCS profiles from a model run in the 2-D mode are also presented for comparison and with the results of the 1-D run. The same OCS boundary conditions were used as for the 1-D run. No additional, detailed sulfur chemistry has been included in the 2-D model at this time (*vide infra.*)

5.3 Model Results

5.3.1 Agreement between the results of the CIT/JPL 1-D and 2-D models and the AER 2-D model

The computed steady-state (total) OCS profile obtained from the 1-D model run has been plotted against the total OCS profiles calculated from analysis of high resolution FTIR spectra taken by the NASA/JPL MkIV instrument over the course of a decade (Figure 6.1). The OCS profiles from the 2-D model are plotted in the same figure along with profiles generated by the AER 2-D model [*Weisenstein et al.*, 1997]. Both models employ recently updated stream functions provided by the Goddard Space Flight Center (GSFC) [*Fleming*, 2002]. Results from the NCAR model are for September at 35 ºN, while the 2-D CIT/JPL model results are from May and from January at 45 ºN and 65 ºN. These altitudes correspond to the latitudes for which MkIV data are available.

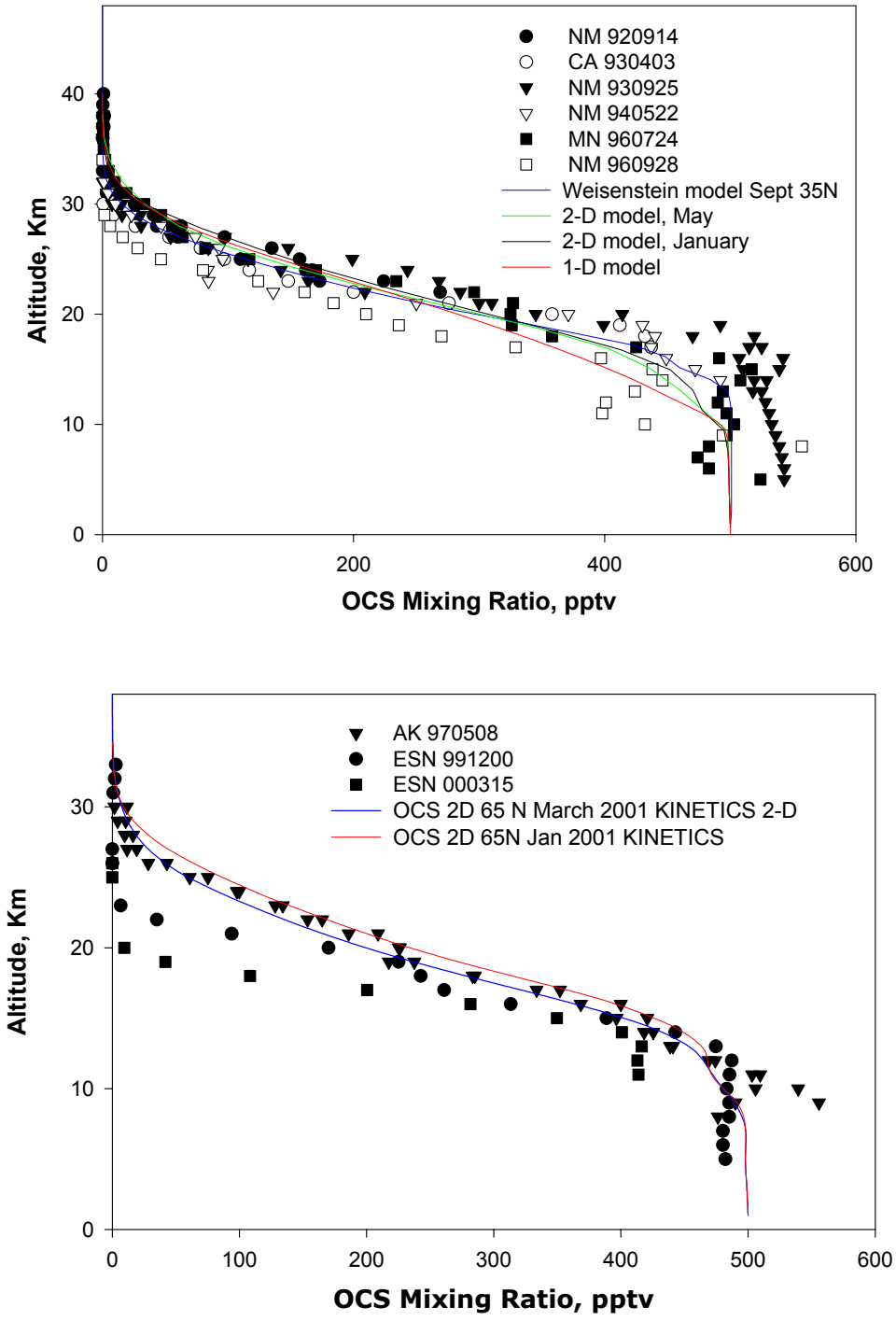

Figure 5.1: OCS profiles from Caltech/JPL KINETICS 1-D and 2-D earth models. The model results have been compared results from 2-D AER model [*Weisenstein*, 2002]. For a a) mid-latitude case and a b) polar latitudes case.

In each case, the altitude that is plotted is the "actual" altitude, which differs somewhat from the tangent altitude shown in Figure 2.1. As noted in Chapter 2, for species that undergoes rapid decay over the altitudes of interest, the tangent altitude, which is the lowest altitude in an altitude bin, is a good approximation of the actual altitude for a given datum. However, the tangent altitude may differ from the actual altitude by several kilometers. In Chapter 2, we used the tangent altitude because we were concerned only with the fraction of OCS lost, and the inversion in the GFIT program that converts tangent altitude data to actual altitude data introduces additional uncertainties.

It could be argued that the 2-D AER model better tracks the observed profiles, especially near the tropopause. This could be due to consideration of convective transport in the tropopause [*Weisenstein et al.*, 1997]. In general, however, there is good agreement between the model predictions and the measured OCS profiles, and among the various models (1-D and 2-D). The exceptions are the MkIV observations from March 2000 from Esrange, Sweden. This dataset is clearly lower than the modeled values for March at a similar latitude (65 ºN), and may be attributed to the exceptionally strong polar vortex of that occurred during the preceding winter.

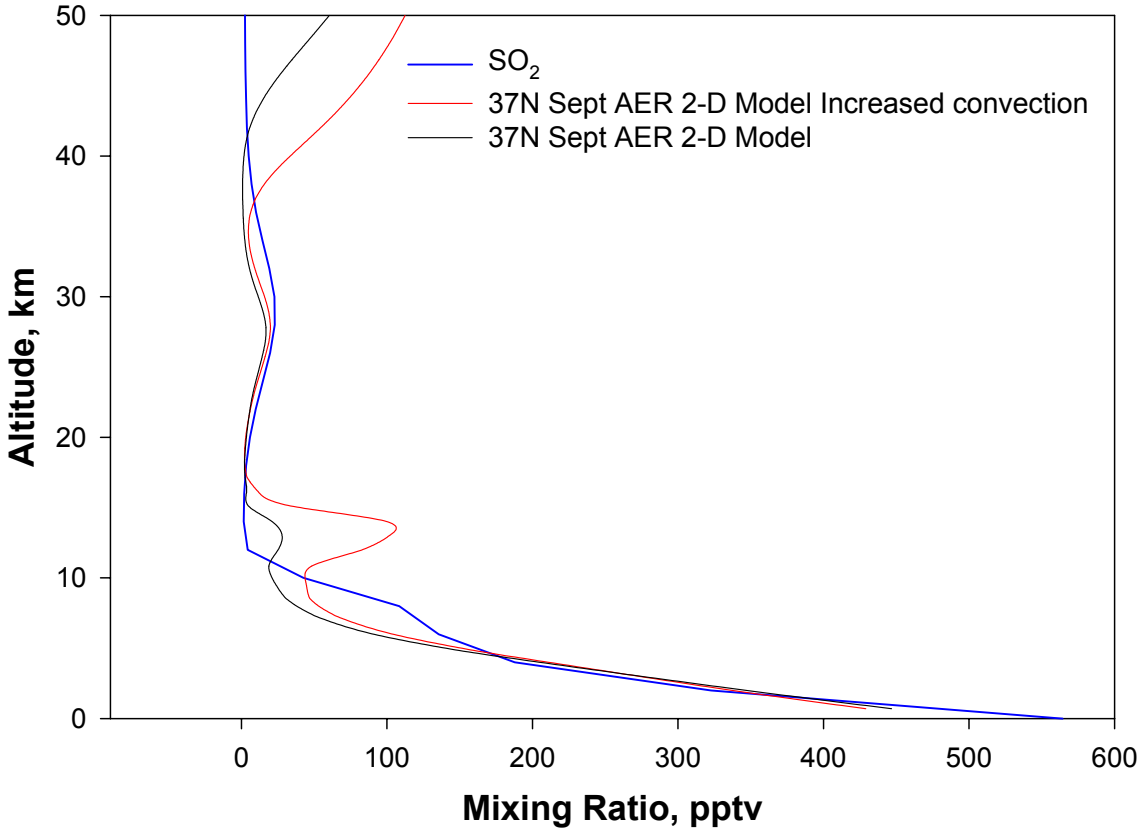

Figure 5.2: SO_2 profile from Caltech/JPL KINETICS 1-D earth model. The model results have been compared to mid-latitude results from 2-D AER model [*Weisenstein*, 2002].

The seasonal variations in the OCS profile at any given latitude are insignificant relative to the large uncertainties in the available data (also see *Chin and Davis* [1995].) The SO_2 profiles from the 1-D model are shown compared to two different mid-latitude SO_2 profiles computed from the 2-D AER model (Figure 5.2). At low altitudes and at altitudes above ~16 km, the results are in good agreement. However, there are significant differences between the profiles between about 5 and 16 km and at high altitudes. The discrepancy between the SO_2 profiles from the KINETICS 1-D and AER 2-D models results from the limitations of a 1-D simulation. The increased SO_2 concentrations in the upper troposphere in the results obtained using the AER model are the result of imposed

conditions of enhanced tropospheric convection, while the differences in the SO_2 profiles at high altitudes arise because H_2SO_4 photochemical decomposition is included in the AER model and is lacking in the Caltech/JPL 1-D model [*Rinsland et al.*, 1995; *Weisenstein et al.*, 1997].

The sulfur mass flux through the tropopause, taken to be the average of the mass flux through 13 km and 15 km (=95 kT-S/y) (Table 5.4) is consistent with the stratospheric sulfate production rate of 71 kT-S/y reported by *Weisenstein et al.* [1997].

Considering the available isotopic data, the good general agreement between our 1-D model and the AER model, and the added computational time of a 2-D model, the 1-D model was used exclusively to explore the isotopic profiles of sulfur species and stratospheric aerosol.

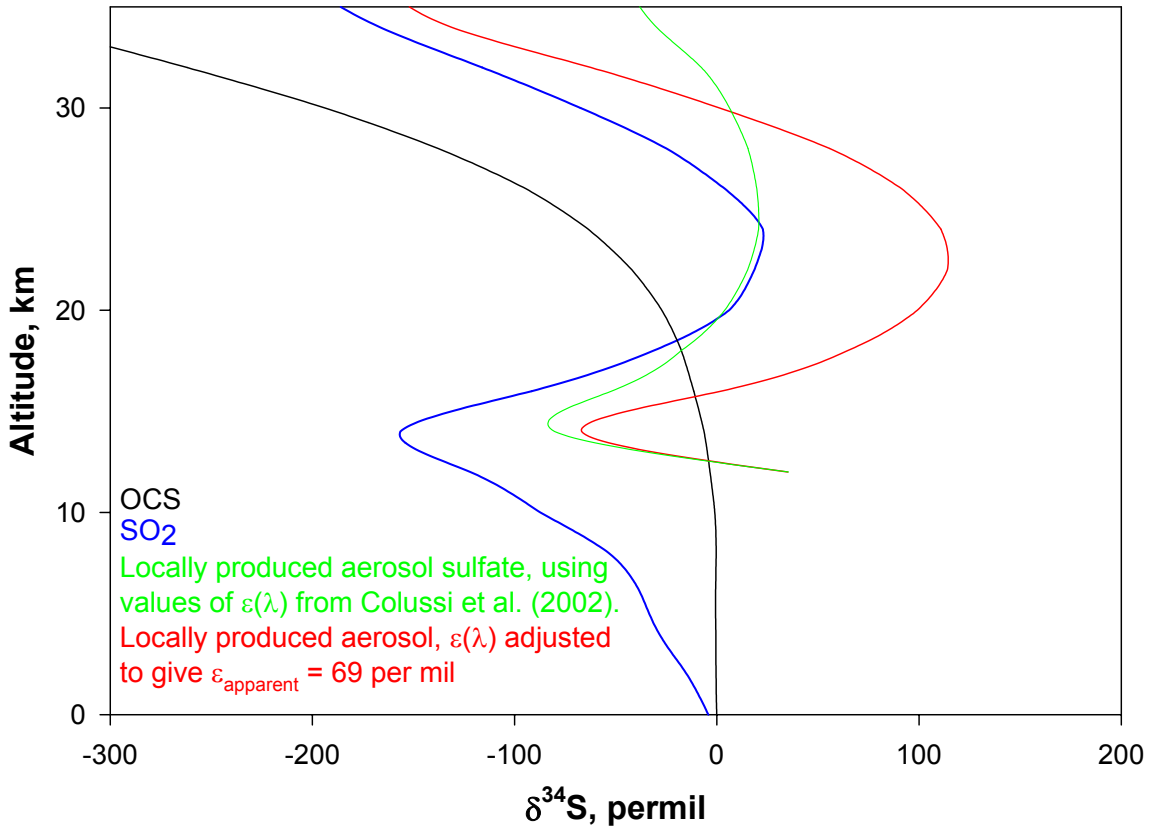

Figure 5.3: Sulfur isotopic composition of locally produced SSA particles and important atmospheric sulfur-containing constituents.

5.3.2 Isotopic enrichment of stratospheric OCS

The computed 1-D $\delta^{34}S$ profile for atmospheric OCS, SO_2 and locally produced SSA particles is shown in Figure 6.3. $OC^{32}S$ absorption cross-sections from *DeMore et al.* [1997] were used in the calculation, while the wavelength-dependent isotopic enrichment factors from Chapter 4 (*vide supra*,) were used to determine the $OC^{34}S$ absorption cross-sections.

A second $\delta^{34}S_{SSA}$ profile was generated by varying the $OC^{34}S$ absorption cross-section by a constant factor so that an $\varepsilon_{apparent}$ of 69‰ was maintained in the lower

stratosphere. This latter value corresponds roughly to the apparent isotopic enrichment factor of 73‰ that was reported in Chapter 2 (see Figure 5.4). When ε is small,

$$\delta = \delta_o + \varepsilon \ln(f) \qquad (6.1)$$

where *f* is the fraction of reactant remaining (OCS in this case). Therefore, the slope of the line represents the apparent isotopic enrichment factor, $\varepsilon_{apparent}$. In Figure 5.4, several different values for $\varepsilon_{apparent}$ are shown, which are superimposed on data from the MkIV flights.

Because dispersion tends to mix air of different ages, the apparent isotopic enrichment factor, $\varepsilon_{apparent}$, is always lower than the actual isotopic enrichment factor ε associated with specific chemical and photochemical loss processes. Simple analytical treatments [*Rahn and Wahlen*, 1997] have been used to estimate a $\varepsilon_{apparent} \sim 0.7\ \varepsilon$. Although atmospheric transport is considerably more complex than characterized in these simplified treatments, we might, therefore, expect ε ~ 150 ‰ on average over the relevant wavelengths on this basis.

More realistically, $\varepsilon_{apparent}$ is a weighted average of the isotopic fractionation of all the OCS loss pathways. Assuming that $\varepsilon_{apparent} = 0.7\ \varepsilon$ because of dispersive effects:

$$1.43\ \varepsilon_{apparent}(z) = f_{ocs+hv}(z)\varepsilon_{OCS\ photolysis}(z) + f_O(z)\varepsilon_O(z) + f_{OH}(z)\,\varepsilon_{OH}(z) \qquad (5.2)$$

where the f_i terms are the fractional contributions of the different OCS loss pathways.

However, at this time, there is no information on the isotopic fractionation associated with OCS oxidation by either O or OH. As mentioned above, we assumed in this model that ε = 0 for these processes. In addition, if we assume that all values of ε are constant over the altitudes of interest, then we obtain:

$$1.43\ \varepsilon_{apparent} = f_{ocs+hv}\varepsilon_{OCS\ photolysis} + f_O\,\varepsilon_O + f_{OH}\,\varepsilon_{OH} = f_{ocs+hv}\varepsilon' + 0 + 0 \qquad (5.3)$$

Therefore, $\varepsilon_{photolysis}$ will be overestimated proportionally to the contribution of OCS oxidation by O and OH and the magnitude of the enrichment factors associated with these processes. For example, if we assume that $\varepsilon_{O\text{-}oxidation} = \varepsilon_{OH\text{-}oxidation} = 73$ ‰, combined with the assertions of *Chin and Davis* [1995] that $f_{O\text{-}oxidation} + f_{OH\text{-}oxidation} = 0.30$, Equation 5.1 yields $\varepsilon' = 117$ ‰, or 20% larger than $\varepsilon_{OCS\ photolysis}$ given the simplifying assumptions of equation 5.3.

We need to emphasize that the values of $\varepsilon_{photolysis}$ used in this study were determined by *Colussi et al.* [2002] at room temperature. Temperature effects are generally expected in $\varepsilon_{photolysis}$. For example, the absorption spectrum of OCS shows a pronounced temperature dependence on the red side of the absorption maximum [*Wu et al.*, 1999]. Therefore, studies of $\varepsilon(\lambda)$ at low temperatures are needed for more accurate analyses, as are independent measurements or calculations of the isotopic enrichment factors for OCS oxidation by O and by OH.

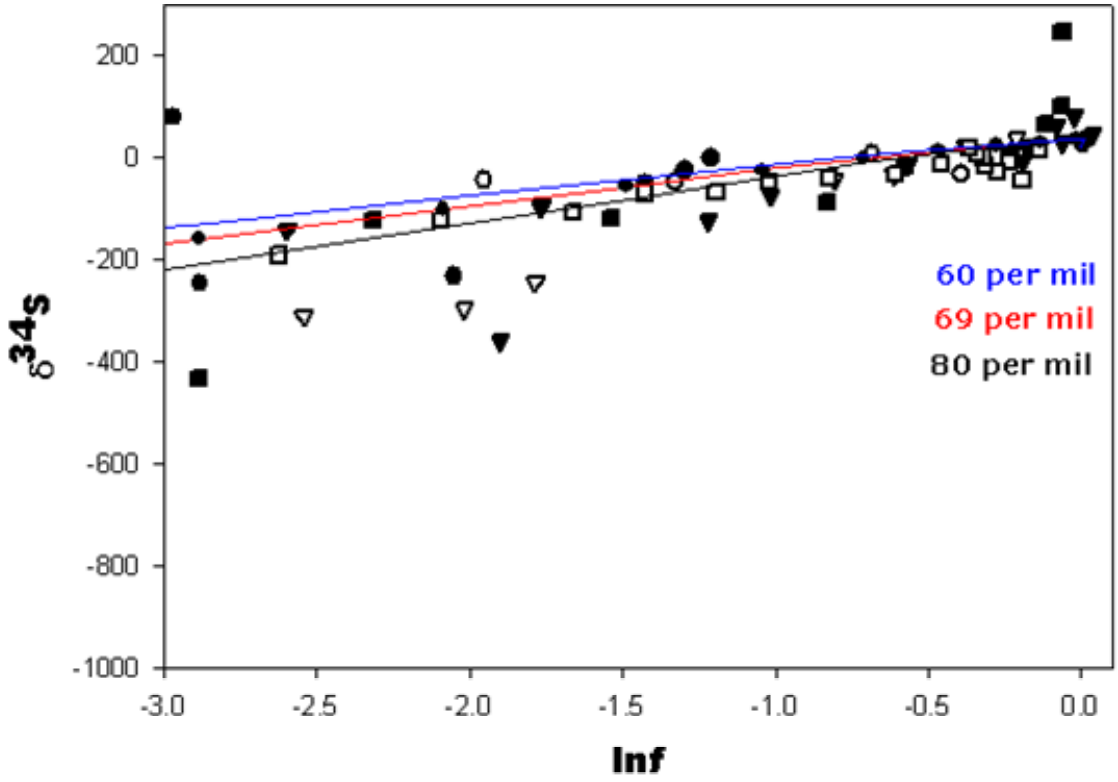

Figure 5.4: Model compared to MkIV data. $\varepsilon_{apparent}$ is found by the slope of the Rayleigh plot analysis (see Chapter 2 and [*Leung et al.*, 2002]).

The isotopic enrichment values given in Table 5.4 show that very large changes in $\varepsilon_{photolysis}$ result in relatively small changes in $\varepsilon_{apparent}$. This suggests that $\varepsilon_{O\text{-}oxidation}$ and $\varepsilon_{OH\text{-}oxidation}$ are relatively large and positive throughout the stratosphere. It is difficult, however, given all the uncertainties in the various model parameters, to determine the values of $\varepsilon_{O\text{-}oxidation}$ and $\varepsilon_{OH\text{-}oxidation}$.

In addition to the the uncertainties in the values of $\varepsilon_{photolysis}$, the value of $\varepsilon_{apparent}$ will depend critically on the manner in which the data has been weighted. In Figure 5.4, several different values of $\varepsilon_{apparent}$ are superimposed on the data from the midlatitude

MkIV flights. The isotopic enrichment values given in Table 5.3 show that very large changes in $\varepsilon_{photolysis}$ result in relatively small changes in $\varepsilon_{apparent}$.

Table 5.3: Adjustment in ε(λ) corresponding to different values of $\varepsilon_{apparent}$

Wavelength, nm	Wavenumber, cm^{-1}	Enrichment (‰)	$\varepsilon_{apparent}$ = 69‰	$\varepsilon_{apparent}$ = 80‰	$\varepsilon_{apparent}$ = 60‰
205	48780	73.8	288.6	342.3	234.9
210	47619	32.3	238.7	290.4	187.1
215	46511	3.5	204.2	254.4	154.0
220	45454	-21.5	174.2	223.2	125.3
225	44444	-24.0	171.2	220.0	122.4
230	43478	-18.3	178.0	227.1	128.9
235	42553	-8.5	189.8	239.4	140.2
240	41667	13.4	216.1	266.8	165.5
245	40816	41.4	249.7	301.8	197.6
250	40000	247.5	497.0	559.4	434.6

In spite of the high level of uncertainties, the average aerosol $\delta^{34}S$ is relatively unaffected by the changes in $\varepsilon_{photolysis}$. On the contrary, it appears that the isotopic composition of SSA particles is dominated by the $\delta^{34}S$ of sulfate produced at low altitudes.

5.3.3 Contribution of SO_2 and H_2SO_4 to the stratospheric sulfate aerosol

Figure 5.5 shows the relative contribution of OCS to stratospheric sulfate aerosol. The overall contribution of OCS to stratospheric sulfate aerosol is 59%, the remaining 41% originating from tropospheric SO_2. The OCS contribution reflects the combined contributions from the oxidation of DMS and CS_2, which are converted to OCS in the troposphere [*Chin and Davis*, 1995] and OCS directly transported to the stratosphere. The SO_2 contribution in the model implicitly includes the contribution from tropospheric sulfate derived from SO_2. *Pitari et al.* [2002] reported a 43% contribution from OCS to

SSA, with 27% arising from SO_2, with tropospheric SO_4^{2-} making up the remainder [*Pitari et al.*, 2002].

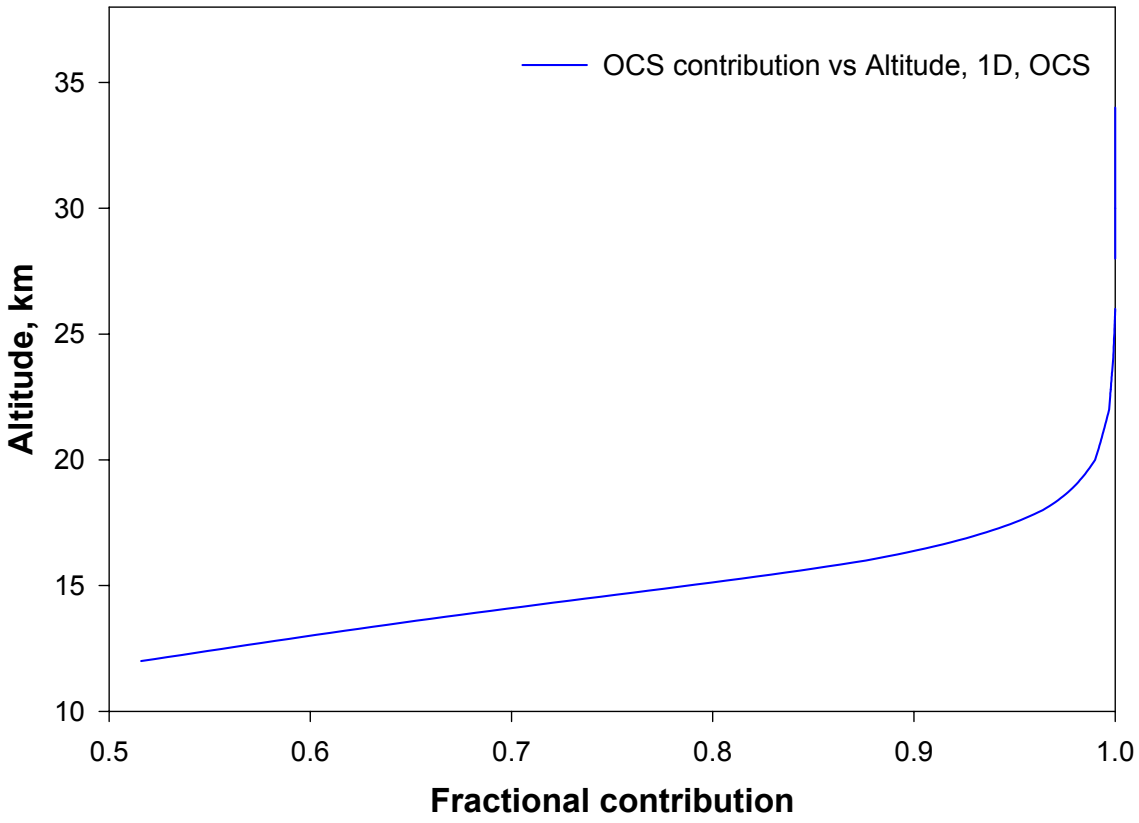

Figure 5.5: Fractional contribution of OCS to the SSA sulfate loading at steady state from 1-D KINETICS model

Figure 5.3 shows the $\delta^{34}S$ profiles of OCS, SO_2, and of sulfate aerosol produced near the tropopause. Aerosol produced close to the tropopause is highly depleted in ^{34}S, while aerosol produced at higher altitudes is enriched in ^{34}S, reflecting the changing relative contributions of SO_2 and OCS at different altitudes (Figure 5.5).

Because ε is > 0 for the oxidation of SO_2 by OH, (the primary homogeneous loss mechanism for SO_2 in the troposphere) SO_2 is increasingly depleted in ^{34}S as it is transported upwards through the troposphere (Figure 5.3). The low $\delta^{34}S$ for sulfate

aerosol produced near the tropopause, therefore, reflects the high relative contribution of SO_2 directly above the tropopause.

At higher altitudes, the $\delta^{34}S$ of the sulfate produced is dominated by the positive and large $\delta^{34}S$ of sulfate from photodissociated OCS. At successively higher altitudes, the $\delta^{34}S$ of the product sulfate reflects the increasingly depleted stratospheric OCS source. A similar trend is observed in SO_2 above the tropopause, which is likewise produced by the photolysis of OCS.

Values of $\delta^{34}S$ of locally produced aerosol are large and positive for most of the stratosphere, and is highly dependent on the values of $\varepsilon_{photolysis}$. However, because of the pressure gradient, the overall $\delta^{34}S_{sulfate}$ is highly weighted towards the values of $\delta^{34}S_{sulfate}$ at lower altitudes. The overall value of $\delta^{34}S_{sulfate}$ for SSA particles is 33 ‰, which is significantly higher than the measured values reported in Appendix A ($\delta^{34}S_{sulfate}$ = 6.8 ‰) or the value ($\delta^{34}S_{sulfate}$ = 2.3 ‰) reported by *Castleman et al.* [1974].

Weisenstein et al. [1997] found that increased convection resulted in a better agreement with the observed aerosol loading. If the SO_2 contribution is actually underestimated in the KINETICS 1-D model, this would bring our results more in line with the results of *Pitari et al.* [2002]. The modeled isotopic composition, $\delta^{34}S$, of stratospheric sulfate is expected to be lower than that in the present model and would therefore reflect the higher contribution of SO_2 and tropospheric sulfate contribution to the total SSA sulfate.

Since the KINETICS model does not treat aerosol microphysics and transport explicitly, it is not possible to determine if the fluxes used in our current model are in fact sufficient to maintain the stratospheric sulfate layer. The loss rate of the sulfur precursors

to the aerosol sulfate is essentially a weighting function to determine the value of $\delta^{34}S_{SSA}$ that accounts for the altitude dependence of aerosol particle lifetimes. In fact, a simple mass flux balance at 13 km gives $\delta^{34}S \sim 20$ ‰ for sulfur species passing through that altitude (Table 5.4). This value is lower than our weighted value for $\delta^{34}S_{Sulfate}$, and closer to measured values. Explicit treatment of aerosol microphysics and transport should reduce some of these uncertainties.

Table 5.4: Sulfur mass balance at 13 km and 15 km altitudes

13 km					
	SO_2	H_2S	H_2SO_4	OCS	Total Flux or Overall $\delta^{34}S$
Flux, molecules/cm^3 s	2.91x10^6	1.04 x10^4	9.78 x10^6	4.77 x10^6	1.75 x10^7 (1.49 x10^2 kT-S/y)
$d^{34}S$, ‰	-86.63	36.86	44.52	35.01	20.06
Fraction of total sulfur species	0.17	~0	0.56	0.27	
15 km					
Flux, molecules/cm^3 s	1.59 x 10^5	4.08 x 10^2	1.38 x 10^3	4.68 x10^6	4.84 x10^7 (4.13 x10^1 kT-S/y)
$d^{34}S$, ‰	-1.11 x 10^2	3.67 x 10^1	3.72 x 10^1	4.34	5.61
Fraction of total sulfur species	0.033	~0	~0	0.97	

Our current model also does not treat heterogeneous chemistry explicitly, so there is no way of determining the relative importance of heterogeneous and homogeneous loss pathways for tropospheric SO_2. The heterogeneous isotopic enrichment factor has been estimated to be ~1.02, (although experimental results have shown a slightly higher value) [*Krouse and Grinenko*, 1991]. This estimate is significantly lower than the values for the homogeneous oxidation of SO_2 under atmospherically relevant temperatures and pressures. If this were true, than the predicted result should be that SO_2 at the tropopause would be less depleted in ^{34}S than our model predicts. On the other hand, the *in situ* production of sulfate, especially at lower altitudes, where aerosol surface area is high and where heterogeneous chemistry should more likely to be important, will be less enriched

in ^{34}S than our model predicts. Again, it is difficult to predict whether this would in fact account for all the discrepancies between the modeled and measured values for $\delta^{34}S_{SSA}$.

As previously noted, a dramatic change in the values of $\varepsilon_{photolysis}$ is required to effect a rather small change in $\varepsilon_{apparent}$. Since the observed $\varepsilon_{apparent}$ = 73 ‰ (Chapter 2) includes the contribution of isotopic fractionation effects of the chemical loss pathways for OCS, the apparent discrepancies between our model predictions and the observed values of $\delta^{34}S_{SSA}$ are unlikely to have arisen from these isotopic effects alone.

5.4 Conclusions

The steady-state results calculated from a simple model 1-D model of the isotopically-independent atmospheric sulfur species show that:

1) SO_2 is highly depleted in $\delta^{34}S$ by the time it reaches the tropopause.

2) $\delta^{34}S$ of sulfate produced in the stratosphere is a function of altitude. The low values of $\delta^{34}S_{SSA}$ seen immediately above the tropopause reflect the importance of a (tropospheric) SO_2 contribution. The OCS contribution to the SSA becomes increasingly more important with increasing altitude.

3) Observed and modeled values for $\delta^{34}S_{SSA}$ differ substantially. Our experimental measurements gave a value for $\delta^{34}S_{SSA}$ of 6.7 ‰; *Castleman et al.* [1974] gave a value of $\delta^{34}S_{SSA}$ of 2.3 ‰, while our 1-D model results predicts an overall value of $\delta^{34}S_{SSA}$ = 33‰.

4) The apparent discrepancy between the measured and modeled results may due to an underestimation of the contribution of the SO_2 and sulfate aerosol.

5) The relative importance of heterogeneous vs. homogeneous transformation of tropospheric of SO_2 may also be an important determinant of the isotopic composition of tropospheric sulfate and SO_2 at the tropopause and thus of SSA sulfur.

6) The observed discrepancy in $\delta^{34}S$ values between model and experiment is unlikely to be due to inaccuracies in parameterization of the isotopic effects associated with stratospheric OCS processing.

7) Inclusion of aerosol microphysics and heterogeneous chemistry/uptake in the model may help to resolve this apparent discrepancy.

8) If 2-D modeling of atmospheric sulfur species is to be more fruitful, a better understanding the geographical distributions of sulfur isotopic compositions is needed. In addition, it is necessary to better characterize the primary convective processes in the troposphere, which may play a crucial role in the exchange of SO_2 and tropospheric sulfate from the troposphere to the stratosphere.

Acknowledgements. We are grateful to Debra Weisenstein (AER) for providing results from her model for direct comparison with our results.

References

Allen, M., Y.L. Yung, and J.W. Waters, Vertical transport and photochemistry in the terrestrial mesosphere and lower thermosphere (50-120 Km), *J. Geophys. Res.*, *86*, 3617-367, 1981.

Burkholder, J.B., M. Mills, and S. McKeen, Upper limit for the UV absorption cross sections of H_2SO_4, *Geophys. Res. Lett.*, *27*, 2493-2496, 2000.

Castleman, J.A.W., H.R. Munkelwitz, and B. Manowitz, Contribution of volcanic sulphur compounds to the stratospheric aerosol layer, *Nature*, *244*, 345-346, 1973.

Castleman, J.A.W., H.R. Munkelwitz, and B. Manowitz, Isotopic studies of the sulfur component of the stratospheric aerosol layer, *Tellus*, *26*, 222-234, 1974.

Chin, M., and D.D. Davis, A reanalysis of carbonyl sulfide as a source of stratospheric background sulfur aerosol, *J. Geophys. Res.*, *100*, 8993-9005, 1995.

Colussi, A.J., F.Y. Leung, and M.R. Hoffmann, Sulfur Isotope Effects on the Ultraviolet Absorption Spectrum of Carbonyl Sulfide. Atmospheric Implications, *Submitted for review*, 2002.

DeMore, W.B., S.P. Sander, D.M. Golden, R.F. Hampson, M.J. Kurylo, C.J. Howard, A.R. Ravishankara, C.E. Kolb, and M.J. Molina, Chemical Kinetics and Photochemical Data for Use in Stratospheric Modeling, pp. 269, JPL/NASA, 1997.

Fleming, E.L., Unpublished results, 2002.

Krouse, H.R., and V.A. Grinenko, editors, *Stable Isotopes: Natural and Anthropogenic sulphur in the Environment, Scope 43*, 400 pp., John Wiley and Sons, 1991.

Leung, F.Y., A.J. Colussi, and M.R. Hoffmann, Sulfur isotopic fractionation in the gas-phase oxidation of sulfur dioxide initiated by hydroxyl radicals, *J. Phys. Chem. A*, *105*, 8073-8076, 2001.

Leung, F.Y., A.J. Colussi, G.C. Toon, and M.R. Hoffmann, Isotopic fractionation of carbonyl sulfide in the atmosphere: Implications for the source of background stratospheric sulfate aerosol, *Geophys. Res. Lett.*, *10.1029/2001GL013955*, 2002.

Notholt, J., Z. Kuang, C.P. Rinsland, G.C. Toon, M. Rex, N. Jones, T. Albrecht, H. Deckelmann, J. Krieg, C. Weinzierl, H. Bingemer, W. R., and O. Schrems, Enhanced upper tropical tropospheric COS: Impact on the stratospheric aerosol layer, *Science*, *300*, 307-310, 2003.

Pitari, G., E. Mancini, V. Rizi, and D.T. Shindell, Impact of future climate and emission changes on stratospheric aerosols and ozone, *J. Atmos. Sci.*, *59*, 414-440, 2002.

Rahn, T., and M. Wahlen, Stable isotope enrichment in stratospheric nitrous oxide, *Science*, *278*, 1776-1778, 1997.

Rinsland, C.P., M.R. Gunson., M.K.W. Ko, D.K. Weisenstein, R. Zander, M.C. Abrams, A. Goldman, N.D. Sze, and G.K. Yue, H_2SO_4 Photolysis - A source of sulfur-dioxide in the upper-stratosphere, *Geophys. Res. Lett.*, *22*, 1109-1112, 1995.

Wang, Y.H., S.C. Liu, P.H. Wine, D.D. Davis, S.T. Sandholm, E.L. Atlas, A. M.A., D.R. Blake, N.J. Blake, W.H. Brune, B.G. Heikes, G.W. Sachse, R.E. Shetter, H.B. Singh, R.W. Talbot, and D. Tan, Factors controlling tropospheric O-3, OH, NOx and SO2 over the tropical Pacific during PEM-Tropics B, *J. Geophys. Res.*, *106*, 32733-32747, 2001.

Weisenstein, D.K., Personal Communication, 2002.

Weisenstein, D.K., G.K. Yue, M.K.W. Ko, N.-D. Sze, J.M. Rodriguez, and C.J. Scott, A two-dimensional model of sulfur species and aerosols, *J. Geophys. Res.*, *102*, 13019-13035, 1997.

Widmann, J.F., and E.J. Davis, Mathematical models of the uptake of $ClONO_2$ and other gases by atmospheric aerosols, *J. Aerosol. Sci.*, *28*, 87-106, 1997.

Wu, C.Y.R., F.Z. Chen, and D.L. Judge, Temperature dependent photoabsorption cross sections of OCS in the 2000-2600 A region, *J. Quant. Spectrosc. Radiat. Transfer*, *61*, 265-71, 1999.

Addendum

In this work, a typical midlatitude case has been considered. In fact, production of stratospheric sulfate may take place primarily in the tropics. This is especially important in light of recent findings of elevated levels of OCS [*Notholt et al.*, 2003] at equatorial latitudes. The profiles of sulfur compounds in the tropics, including those of SO_2, OCS, and DMS, maybe considerably different from those in the subtropics. The corresponding isotopic profiles would also be expected to be different because the isotopic composition of a compound depends on its extent of reaction as well as on the conditions under which it is processed. This is not particularly important in the case of OCS, which is not significantly processed in the troposphere, although the suggestion that these elevated OCS may be the product of biomass burning rather than from direct biogenic sources highlight the need for direct measurements of isotopic compositions as well as for studies of the isotopic fractionation effects of oxidative reactions. However, the case for short-lived (tropospheric) species such as SO_2 is markedly different. Unfortunately, measurements of tropical SO_2 mixing ratio profiles are rather sparse, and are available only up to 12 km, several kilometers under the tropical tropopause [*Wang et al.*, 2001], limiting the usefulness of detailed modeling studies.

In order to estimate the influence of varying tropical SO_2 profiles on the sulfur isotopic composition of SSA particles, we considered two cases, the first where the fraction of SO_2 remaining, $f = 0.40$ and $f = 0.60$ at the tropopause. Assuming that the average value for the isotopic enrichment factor for $SO_2 + OH$ of ε=140‰, we estimated that the SO_2 that reaches the tropopause have values of $\delta^{34}S_{SO2}$ of -128‰ and -72‰, respectively. Further assuming that all of the SO_2 reaching the tropopause in fact is

uplifted into and oxidized completely in the stratosphere, and the $\delta^{34}S = 80‰$ for sulfate produced from oxidation [*Leung et al.*, 2002], uplifted SO_2 would have to account for 38 to 53% of the total sulfate, which are generally in agreement with our results from the midlatitude run. Given the uncertainties in the current model parameters, it is expected that the results of a one dimensional model of sulfur species in the tropics or of a 2-D model would not differ qualitatively from the results presented here.

Appendix A.5.1: Input and Output for the JPL/Caltech 1-D KINETICS model

The input and program files used in our run of the 1-D and 2-D KINETICS model are archived on a Caltech workstation, MERCU1, which operates on a VMS operating system, as is maintained by the Division of Geological and Planetary Sciences by the laboratory of Professor Yuk Yung.

All files used in the 1-D model are located in USER1:[fyl.trial] and its subdirectories. The core input file is KINEARTH8JPL00.INP-130KM, which contains critical run parameters including number and size of time steps, the species that will be modeled, and planetary parameters. The file ATMOS30JPL97V8.INP contains the initial profiles of all the species, including temperature and pressure profiles. The boundary conditions used in the program are found in KINEARTH8-BOUND.INP. The rate constants for all the chemical reactions used in the model, including those for the sulfur isotopic chemistry are found in KINDAT3EARTH.INP-JPL00. The recommendations of DeMore et al. (1997) are used unless otherwise stated.

The photochemical cross-sections used in the model are contained in a separate subdirectory: USER1:[fyl.trial.crossdisk]. The CROSSDISK.INP-JPL00 file contains cross-sections following the recommendations of *DeMore et al.* [1997].

The program is run via a series of batch command files. CROSSDISK.COM and KINDATA3.COM must be run before KINEARTH8JPL00.COM if any changes have been made in either the absorption cross-sections or chemical rate constants, respectively.

The general library is KINETGEN8V4X.LIB, which contains all the default subroutines. The program first refers to a custom library: KINEARTH8JPL00.LIB

before going to the default subroutines. In the implementation used here, the custom code was modified to include rainout rates for $SO_{2(g)}$ and $H_2SO_{4(g)}$.

The output of the CROSSDISK.COM and KINDATA3.COM are CROSSDISK-USE.INP-JPL00, KINDATA3.OUT, and KINDAT3EARTH.PUN-JPL00. The *.PUN files serve as input for the main program. The results of the model run are reported in KINEARTH8JPL00.OUT-130KM.

Appendix A.5.2: Input for the 2-D model

The input files for the 2-D implementation of the model can be accessed from USER1:[fyl.2d]. The command file is named KINOCS.com, and the core input file is named KINOCS.INP. The 2-D model has the additional complication of the transport functions changing monthly. Otherwise, analogous input and output files exist for the 2-D as the 1-D implementation of the program. At present, only the chemical and photochemical pathways involving OCS have been implemented.